Systems & Control Transactions

Research Article
Foundations of Computer Aided Process Design (FOCAPD 2024)
Breckenridge, Colorado, USA. July 14-18, 2024
Peer Reviewed Conference Proceeding

PSE PRESS

Optimal Design of Antibody Extraction Systems using Protein A Resin with Multicycling

Fred Ghanem[a], Purnima M. Kodate[b], Gerard M. Capellades[a], and Kirti M. Yenkie[a]*

[a] Rowan University, Department of Chemical Engineering, Glassboro, NJ, USA
[b] Department of Pathology, Government Medical College, Nagpur, India
* Corresponding Author: yenkie@rowan.edu.

ABSTRACT

Antibody therapies are important in treating life-threatening ailments such as cancer and autoimmune diseases. Purity of the antibody is essential for successful applications and Protein A selective resin extraction is the standard step for antibody recovery. Unfortunately, such resins can cost up to 30% of the total cost of antibody production. Hence, the optimal design of this purification step becomes a critical factor in downstream processing to minimize the size of the column needed. An accurate predictive model, as a digital twin representing the purification process, is necessary where changes in the flow rates and the inlet concentrations are modeled via the Method of Moments. The system uncertainties are captured by including the stochastic Ito process model of Brownian motion with drift. Pontryagin's Maximum Principle under uncertainty is then applied to predict the flowrate control strategy for optimized resin use, column design, and efficient capturing of the antibodies. In this study, the flow rate is controlled to optimize the process efficiency via maximizing the theoretical plate number with time, the objective for efficient resin usage within a fixed-size column. This work successfully achieved optimality, which was also confirmed via experimentation, leading to higher antibody resin loading capacity. When the work was expanded to 200 cycles of Protein A usage, significant improvements in the downstream process productivity were achieved allowing for smaller footprint columns to be used.

Keywords: Optimization, Dynamic Modeling, Stochastic Optimization, Model Reduction, Antibody Extraction.

INTRODUCTION

Antibodies are produced by many pharmaceutical companies to treat various autoimmune diseases [1]. Unfortunately, up to 30% of the production cost of the antibody [2] is based on a single purification step, the Protein A resin, that selectively captures the antibody from the fermentation broth with up to 99% purity. Therefore, the optimal usage of such an expensive resin is necessary. Since the cost of antibody production depends on the cost of this resin, an optimal control strategy is needed to maximize the efficient use of the resin as seen in Figure 1 giving the possibility to use smaller systems.

The effluent concentration of the expensive capture step will also follow a sigmoidal function [3] as seen in Figure 1. With many sigmoidal models used to evaluate packed bed systems [4], the model parameters are highly dependent on flow rates and inlet concentrations [5].

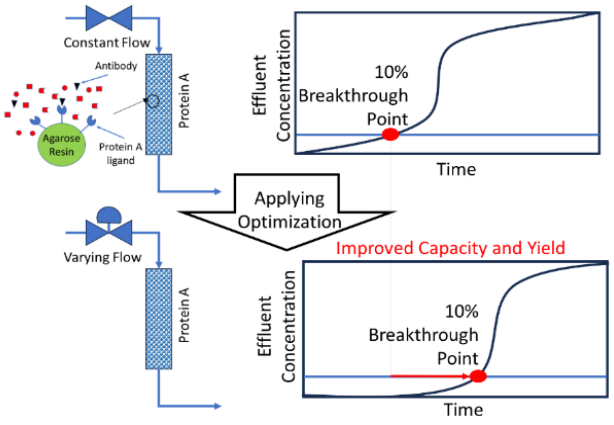

Figure 1. Optimal design and operating policy for the Protein A resin step in antibody extraction.

A generalized fixed bed model can be used where the parameters are defined by their relationships to the flow rate and inlet concentration [4]. Pontryagin's maximum principle [6] defines our purification system as requiring an optimization strategy via adjustments of controllable process variables such as flow rate.

To accomplish such optimality, the method of moments is used to simplify the system as a univariate function of time [7]. However since the moments are typically used to represent chromatographic steps [8] with a population distribution curve, the Protein A capture step cumulative curve will need to be transformed via its derivative into a distribution curve (as shown in Figure 2). The Hamiltonian function [9] is then formulated using moments as state variables and introducing adjoint variables to define the path taken during the optimization via maximizing the theoretical plate number [10] for the most efficient use of the resin.

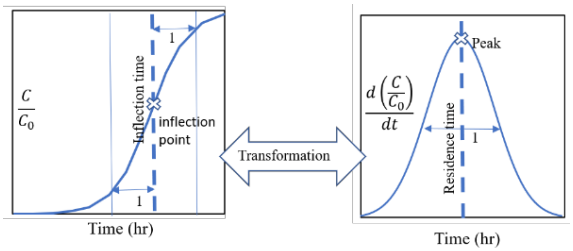

Figure 2. Sigmoidal function transformation from a cumulative to a distribution curve via its derivative.

Since the inlet concentrations and model parameters can vary during production, capturing such uncertainties during optimization is important. The stochastic Ito process [11] was picked to capture the variability of the system. The purpose of this work is to confirm that varying the flow rate with time maximizes the resin performance over using fixed flow rates, a standard practice in existing industrial chromatography column operations [12]. While some industries adopted continuous chromatography [13], such as the use of simulated moving beds [14], to maximize the efficient use of the resin, considerable investments in such complex systems are required [15]. The novelty of our approach lies in its simplicity in maximizing the system performance of a single-column system avoiding the high cost of a continuous system.

METHODOLOGY

The procedure consists of feeding IgG4 antibody [16] through 1 ml of packed Minichrom column (supplied by Repligen) packed with Praesto Jetted A50 Protein A resin (supplied by Purolite). Three different concentrations of the antibody (2, 5, and 7 mg/ml) were used at 4 different residence times (3, 4.8, 6, and 10 min). A standard sigmoidal function [17], predicting the column output is seen below.

$$\frac{C}{C_0} = \frac{1}{1+\exp(a - \mathrm{b}\, t)} \quad (1)$$

where C_0- inlet concentration, C - effluent concentration varying with time, a and b – empirical parameters of the sigmoidal function, and t– time. The model can be further modified into a modified Yoon-Nelson equation [18] where $t_{\frac{1}{2}}$ – time needed to get to $C/C_0 = 1/2$.

$$\frac{C}{C_0} = \frac{1}{1+exp\left(b\left(\frac{a}{b} - t\right)\right)} = \frac{1}{1+exp\left(b\left(t_{\frac{1}{2}} - t\right)\right)} \quad (2)$$

The parameters in the model can be calculated by minimizing the Sum of Squares of the Error (SSE) between model predictions and experimental measurements[19]. Since the sigmoidal function is represented by a cumulative curve, it is necessary to transform Eq. 2 into a distribution curve, closely depicting chromatographic separations[20]. Such a transformation is achieved by taking the derivative of the sigmoidal model, $d(\mathrm{C}/\mathrm{C}_0)/dt$.

The Method of Moments

The general form of the truncated temporal moments [21] used in chromatographic separations is defined by the following equation [22]:

$$\mathrm{m_i} = \int_0^t t^i \frac{\mathrm{d}\left(\frac{\mathrm{C}}{\mathrm{C_0}}\right)}{\mathrm{dt}}\, dt \quad (3)$$

Eq. 3 is the basic form to present the 4 moments describing our system [23]. In chromatographic operations, the truncated temporal moment equations are represented as follows [24]:

$$\text{Zeroth moment} = \mathrm{m_0}(t) = \mu_0(t) = \int_0^t \frac{d\left(\frac{C}{C_0}\right)}{dt}\, dt = \frac{\mathrm{C}}{\mathrm{C_0}}(t) = y_{1(t)} \quad (4)$$

$$\text{First normalized moment} = \mu_1(t) = \frac{\int_0^t t\frac{d\left(\frac{C}{C_0}\right)}{dt}dt}{\int_0^t \frac{d\left(\frac{C}{C_0}\right)}{dt}dt} = \frac{\int_0^t t\frac{d\left(\frac{C}{C_0}\right)}{dt}dt}{\mu_0(t)} = \mathrm{t_m}(t) = y_{2(t)} \quad (5)$$

$$\text{Second central normalized moment} = \mu_{2c}(t) = \frac{\int_0^t (t-\mu_1)^2\frac{d\left(\frac{C}{C_0}\right)}{dt}dt}{\mu_0(t)} = \sigma^2(t) = y_{3(t)} \quad (6)$$

$$\text{Third central normalized moment} = \mu_{3c}(t) = \frac{1}{\mu_{2c}^{1.5}}\frac{\int_0^t (t-\mu_1)^3\frac{d\left(\frac{C}{C_0}\right)}{dt}dt}{\mu_0(t)} = s^3(t) = y_4(t) \quad (7)$$

where t_m – column residence time or the time needed to reach the maximum peak, σ^2 – variance or square of the standard deviation, and s^3 – skewness cubed.

Capturing Uncertainties

As uncertainties can affect the protein A resin performance leading to inefficient removal of the antibodies, it is necessary to account for these variations via the adoption of stochastic process equations and models [25]. One of the simplest stochastic process models is the Brownian motion / Wiener process [26], where one begins at a known initial value and takes equiprobable

steps in any direction [27]. An example of the Brownian motion method is the Ito process with drift [28] defined below as a modified Euler step.

$$y_t = y_{t-\Delta t} + \alpha\,\Delta t + \kappa\,\varepsilon\,(\Delta t)^{1/2} \quad (8)$$

where y_t – the moment at time t, $y_{t-\Delta t}$ – the moment at time t - Δt, α – Ito process drift parameter, κ – Ito process deviation parameter, ε – random number with a normal distribution of zero as the mean and a standard deviation of 2, and Δt – time step. The Ito process has been applied to other modes of purification such as crystallization [29] and distillation [30].

Objective function and boundary conditions

Figure 3 demonstrates that an increase in the normalized first moment, t_m, results in more antibody extraction, while a decrease in the second central moment, σ^2, results in lower leakage. Therefore, the objective would be to maximize t_m and minimize the variance σ^2. In chromatography, better purification is achieved when the theoretical plate number (TPN) is maximized [31].

$$TPN = \frac{t_m^2}{\sigma^2} \quad (9)$$

The objective, J_{max}, is to maximize the theoretical plate number.

$$J_{max(Q)} = max\left(\frac{t_m^2}{\sigma^2}\right) = max\left(\frac{\mu_1^2}{\mu_{2c}}\right) \quad (10)$$

The maximum value is achieved when the derivative of the objective function is equated to zero.

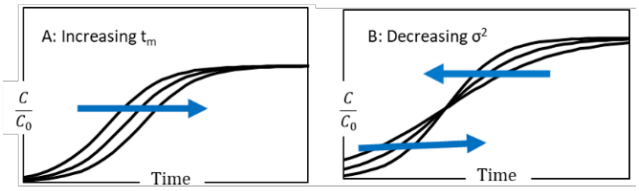

Figure 3. Effect of increasing the residence time (A) compared to decreasing the variance (B).

Optimal Control

To simplify the optimization approach, we can linearize the four stochastic moments into a single Hamiltonian function as follows[25]:

$$H = \sum_{i=1}^{4} [z_i F_i + \omega_i \frac{g_{y_i}^2}{2}] \quad (11)$$

where H – Hamiltonian function, z_i – adjoint variable, F_i – differential changes of the state variable with time = $\frac{dy_i}{dt}$, ω_i – stochastic adjoint variable, and $g_{y_i} = \sqrt{\frac{var(\Delta y_i)}{\Delta t}}$ (12)

The adjoint variables limit the pathways to achieve the objective and are defined by their derivatives:

$$\frac{dz_i}{dt} = -\sum_{k=1}^{4} [\frac{\partial F_k}{\partial y_i} z_k + \frac{1}{2}\frac{\partial g_k^2}{\partial y_i}\omega_k] \quad (13)$$

$$\frac{d\omega_i}{dt} = -\sum_{k=1}^{4} [2\omega_k \frac{\partial F_k}{\partial y_i} + \frac{\partial^2 F_k}{\partial y_i^2} z_k + \frac{1}{2}\frac{\partial^2 g_k^2}{\partial y_i^2}\omega_k] \quad (14)$$

Pontryagin's maximum principle (PMP) is used to apply the optimal control strategy [32] to our antibody extraction system. PMP utilizes the Hamiltonian by imposing the optimality conditions for the objective function [33]. Another optimization method that could be used is the orthogonal collocation method [34]. The collocation numerical method would simplify our optimization strategy for our deterministic approach [35] but is challenging when dealing with uncertainties captured in the Hamiltonian function used in the PMP method.

Optimal control is applied using a manageable system parameter such as the flow rate. Derivatization of the Hamiltonian function to the flow rate (Q) can be represented by its coordinates (the state and the adjoint variables) using the following expression[29] of a derivative chain rule:

$$\frac{dH}{dQ} = \sum_{i=1}^{4} \frac{dH}{dy_i}\frac{dy_i}{dQ} + \sum_{i=1}^{4} \frac{dH}{dz_i}\frac{dz_i}{dQ} + \sum_{i=1}^{4} \frac{dH}{d\omega_i}\frac{d\omega_i}{dQ} \quad (15)$$

Eq. 15 defines the Hamiltonian gradient where the gradient is nullified when flow rate changes are no longer necessary. The integrations were done using the Euler steps[29]. The initial values of the state variables are obtained from the starting point, and the final values of the adjoint variables (z and ω) are obtained from the optimal objective for the purification system.

Optimal Control Solution Strategy

The pump flow rate is bound between 2 flow rates corresponding to residence times of 3 and 10 min in our experimental work. Considering that the inlet antibody concentration enters at 5 mg/ml, the flow rate, initially set at the slow residence time of 10 min, is expected to change to optimize the extraction of the antibody.

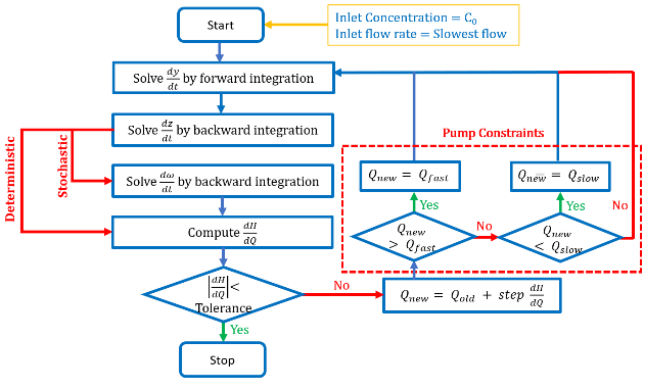

Figure 4. Flowchart for stochastic optimal control.

Figure 4 summarizes the algorithm using Matlab as the optimization tool for the deterministic and stochastic approach[36]. The main difference between the two

approaches is the bypass loop to calculate the stochastic adjoint variable ω. Figure 4 demonstrates how our state and adjoint variables are calculated before calculating the Hamiltonian gradient which is compared to the tolerance picked for the system. Depending on the Hamiltonian gradient value, the optimization would be achieved (below the tolerance) or the flow rate would be adjusted (above the tolerance) between the two flow rate boundaries for another iteration.

RESULTS

The experimental data for the concentration ratio of antibody igG4 with time from a 1 ml Minichrom column packed with Praesto Jetted A50 resin is seen in Table 1.

Table 1: Experimental data.

Inlet Concentration C_0 = 2 mg/ml			
Residence time (min)	Time to C/C_0 = 0.05 (min)	Time to C/C_0 = 0.10 (min)	Time to C/C_0 = 0.50 (min)
3	82.7	90.6	135.2
4.8	157.6	170.3	216.9
6	198.3	216.8	271.3
10	334.8	364.6	456.2
Inlet Concentration C_0 = 5 mg/ml			
Residence time (min)	Time to C/C_0 = 0.05 (min)	Time to C/C_0 = 0.10 (min)	Time to C/C_0 = 0.50 (min)
3	31.5	35.3	57.9
4.8	61.4	67.8	97.8
6	87.4	94.2	123.6
10	162.8	173.2	209.2
Inlet Concentration C_0 = 7 mg/ml			
Residence time (min)	Time to C/C_0 = 0.05 (min)	Time to C/C_0 = 0.10 (min)	Time to C/C_0 = 0.50 (min)
3	23.7	24.9	30.2
4.8	40.9	42.6	49.4
6	52.0	54.1	62.0
10	87.7	92.5	104.9

We extrapolated the sigmoidal model parameters via the minimization of the SSE (sum of square errors). These parameters are summarized in Table 2 as they vary with changes in inlet concentration and flow rate.

Table 2: The sigmoidal function parameters.

Residence Time (min)	Concentration (mg/ml)	Empirical parameter $t_{1/2}$ (min)	Empirical parameter b (min^{-1})
3	2	135.1	0.0519
4.8	2	217.1	0.0480
6	2	271.4	0.0403
10	2	455.8	0.0241
3	5	57.8	0.1031
4.8	5	97.8	0.0762
6	5	123.5	0.0772
10	5	209.2	0.0619
3	7	30.2	0.4317
4.8	7	49.4	0.3344
6	7	61.9	0.2849
10	7	105.0	0.1748

From Table 2, we extrapolate the relationships between the model parameters and system characteristics.

$$t_{\frac{1}{2}} = 82.81\, RT \exp(-0.295\, C_0) \quad (16)$$

$$b = \frac{1}{-0.57\, RT\, C_0 + 4.49\, RT - 1.12\, C_0 + 9.08} \quad (17)$$

where RT – residence time = RV/Q , and RV – resin volume in the column. The results comparing the empirical parameters with the calculated data from Eq. 16 and Eq. 17 are summarized in Table 3. It displays that the fluctuations in the parameters $t_{\frac{1}{2}}$ and b are within ±10% and ±20% respectively.

Capture Uncertainty via Stochastic Processes

When considering an inlet antibody concentration that fluctuates 10% around 5 mg/ml and capturing the parameter fluctuations described by Table 3, we can display the effect of these uncertainties on the 4 moments.

Table 3: Results of the sigmoidal function parameters for calculated versus empirical.

Residence Time (min)	Concentration (mg/ml)	Empirical parameter $t_{1/2}$ (min)	Empirical parameter b (min^{-1})	Calculated parameter $t_{1/2}$ (min)	Calculated parameter b (min^{-1})	Percent difference on $t_{1/2}$	Percent difference on b
3	2	135.1	0.0519	137.7	0.0592	-1.9	-14.1
4.8	2	217.1	0.0480	220.3	0.0436	-1.5	9.1
6	2	271.4	0.0403	275.4	0.0371	-1.5	7.9
10	2	455.8	0.0241	459.0	0.0248	-0.7	-2.9
3	5	57.8	0.1031	56.8	0.1190	1.7	-15.5
4.8	5	97.8	0.0762	90.9	0.0881	7.0	-15.6
6	5	123.5	0.0772	113.7	0.0751	8.0	2.8
10	5	209.2	0.0619	189.5	0.0503	9.4	18.7
3	7	30.2	0.4317	31.5	0.3650	-4.4	15.5
4.8	7	49.4	0.3344	50.4	0.2747	-2.1	17.8

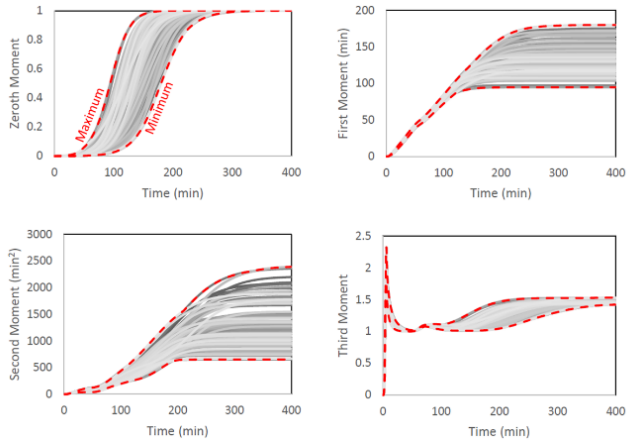

Figure 5. Static uncertainty (100 scenarios via sampling) manifested as Dynamic uncertainty.

Figure 5 shows the effect of static uncertainties in the initial condition or process parameters manifesting as dynamic uncertainties in all the state variables (i.e. the 4 moments with respect to time). Figure 6 demonstrates that the Ito process of Brownian motion with drift can capture the dynamic uncertainties of the 4 moments.

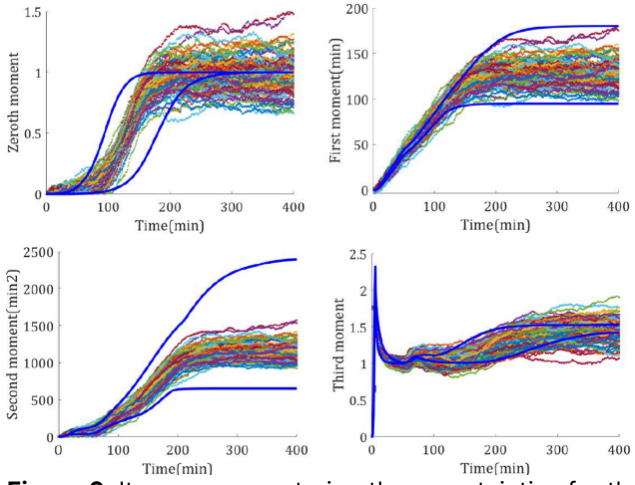

Figure 6. Ito process capturing the uncertainties for the four moments.

Results from Stochastic Optimal Control

We run the Matlab flowchart program seen in Figure 4, for over 40,000 iterations to achieve the optimal flow rate path. While the state variables, y_i, are integrated in the forward direction from the initial conditions, [y_1(0) 0 0 0], the adjoint variables, z_i and ω_i, are integrated in a backward direction from the final conditions, $[0 \quad (2\mu_1(tfinal))/(\mu_{2c}(tfinal)) \quad -\left(\mu_1^2(tfinal)\right)/(\mu_{2c}^2(tfinal)) \quad 0]$ and [0 0 0 0], respectively based on the final optimum of Eq. 11. We use Euler's method for integration with a very small-time step. At each time step, the values of the Hamiltonian and its derivative are calculated.

Two approaches were evaluated: a deterministic approach, ignoring the uncertainties, and a stochastic approach. During each of the iterations, the flow rate is adjusted until the optimal flow is achieved. Figure 7 displays the changes in the flow rates during the deterministic optimal control approach. It shows that deterministic optimal flow control will start by increasing the flow towards the maximum flow to get as much product processed before it reduces the flow to avoid early antibody breakthrough.

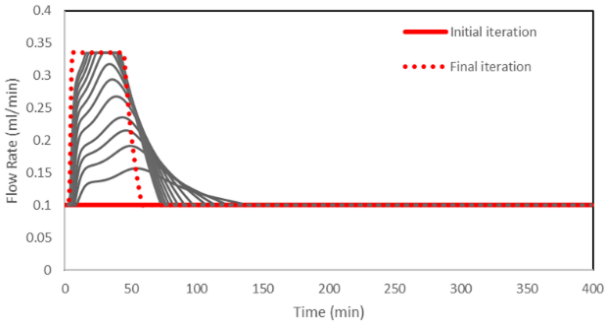

Figure 7. Iterations of the flow rate to achieve deterministic optimal control.

Experimental Validation of Optimal Control

From Figure 8, Both the stochastic optimal flow and the deterministic optimal flow will adjust to the maximum flow rate initially before reducing it to minimum flow rate around 70 minutes. The deterministic optimal flow decreases slightly earlier to the slow flow rate of around 60 minutes. Since running the process at the fast flow rate initially followed by a slowdown improved the process performance, we ran an experiment to confirm the improvement by manually changing the flow from the fastest flow rate to the slowest flow rate after $C/C_0 = 0.05$ is reached.

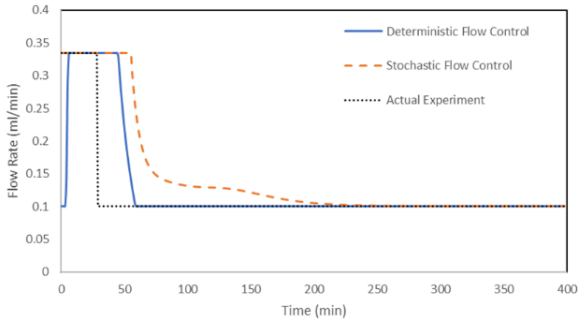

Figure 8. Optimal flow control for both deterministic and stochastic approaches with manual flow rate adjustment.

Table 4 demonstrates the effectiveness of using an optimal flow rate to maximize the antibody extraction over using a constant flow rate. Both stochastic and

deterministic approaches succeeded in improving the system performance by extracting more antibodies in less time than a fixed slow flow rate. The actual experiment also demonstrated an improvement in antibody extraction over running at a constant flow rate. While the experimental manually controlled work did not duplicate the data obtained from the deterministic or the stochastic approach, the results confirmed that designing targeted operating policies such as the fast flow followed by decreased flow later in the process, will achieve more antibody extraction.

Table 4: Optimal control results versus constant flow.

Conditions	Max Flow	Min Flow	Deterministic	Stochastic	Actual test
Antibody Extracted to C/Co = 0.1 mg (mg antibody/ml resin)	65.0	73.6	97.1	105.7	105.3
Antibody Extracted to C/Co = 0.5 mg (mg antibody/ml resin)	86.0	92.9	112.8	122.6	113.4

When checking the amount of antibody extracted until 10% breakthrough, Table 4 demonstrates that the flow rate adjustment used in the experimental validation resulted in 43% more antibody removed than using the slowest flow rate setting. This validated improvement in the resin capacity leads to efficient utilization of the expensive Protein A resin. As the system residence time is influenced by the size of the column used, the optimization allows for the efficient utilization of any size resin column within the limitations of the system flow rates.

Multicycle Optimization

Since the Protein A resin is the most expensive step in the downstream processing of antibodies, cycling it for multiple uses is necessary to get the most value out of its resin life. But with every cycle, the Protein A resin will degrade due to caustic cleaning or due to fouling from the various molecules in the fermentation broth.

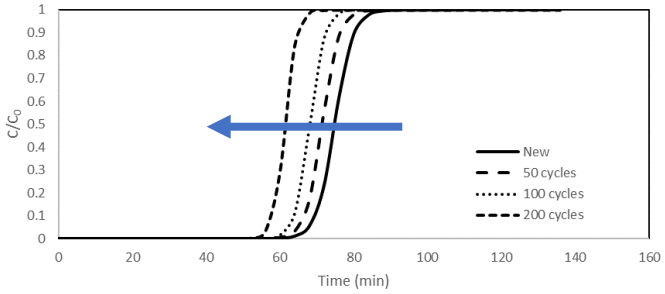

Figure 9. Protein A resin degradation during multicycle operations at 6 min residence time.

Figure 9 shows the actual effect of Protein A degradation during multiple cycles as the breakthrough tends to occur sooner in late cycles (also called life time study). For example, the time to reach 50% breakthrough dropped from 75 min to 68 minutes after 100 cycles. While the model parameters change with contact time and inlet concentration (as seen in equations 20 and 21), further modification of these parameters can be made to depict the degradation with each cycle. Therefore, it is expected that optimal flow rate pathways might be different as the resin degrades.

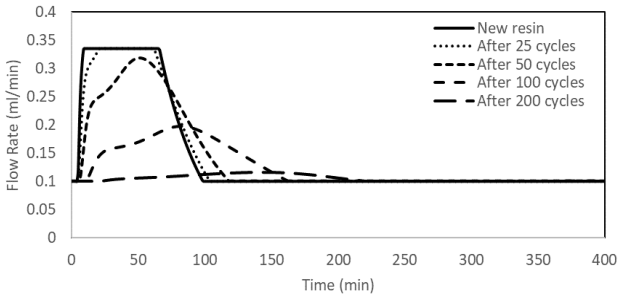

Figure 10. Optimal flow rate during multicycle use

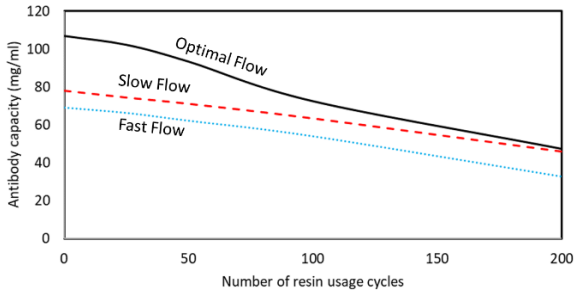

Figure 11. Effect of resin degradation on the optimal flow

Figure 10 confirms that hypothesis showing that the system will not be running at the high flow rates for as long as when using a newer resin. At the end of the 200 cycles, the optimal flow rate is to keep the flow constant at its lowest setting. Figure 11 confirms that the optimal flow rate will get closer to the slowest flow rate as the number of cycles increases. Once optimal conditions cannot be improved beyond running at the slowest flow rates, resin replacement becomes the next logical step.

Table 5 summarizes the effect of using the optimal flow rate over 200 cycles of Protein A resin usage. Table 5 demonstrates that over 20% increase in cumulative binding capacity, over 30% savings on cycle time, and over 80% in productivity can be achieved during the 200-cycle life of the Protein A resin. The impact of such improvement allows the use of any size column while avoiding system overdesign usually necessary for similar results. An 84% improvement in productivity translates to using 46% less resin to get the same performance as the slowest flow rate and therefore 46% less footprint. In addition, reducing the loading time by 34% allows the extracted antibody to have less contact time with the host

cell proteins containing the damaging enzymes that can reduce the process yield [37].

Table 5: Performance Improvement in the Resin Usage Capacity over 200 Cycles.

Dynamic binding capacity (total grams/ml-resin)	C/C_0 = 10%	C/C_0 = 50%
Optimal control for 200 cycles	15.2	19.6
Constant low flow at residence time = 10 min for 200 cycles	12.5	16.8
% Improvement over 200 cycles	21.6	16.7
Total time of loading production needed (hours)		
Optimal control for 200 cycles	351	565
Constant low flow at residence time = 10 min for 200 cycles	531	772
% Improvement (200 cycles)	33.9	26.8
Productivity (total grams/liter-resin-hour)		
Optimal control for 200 cycles	43.3	34.7
Constant low flow at residence time = 10 min for 200 cycles	23.5	21.8
% Improvement over 200 cycles	84.2	59.2

CONCLUSIONS

Protein A resins are the most expensive step in the manufacturing of critical antibody therapies. Successful control strategies become necessary to maximize the efficiency of resin usage in downstream processing. When applying optimal control strategies via flow rate adjustment, we demonstrated through prediction at first and then confirmed through experimentation that optimal design is achieved by varying the flow rates rather than using a fixed flow rate. Optimality is achieved by initially running the resin column at high flow rates to get as much feed processed before reducing the flow to avoid an early breakthrough. During the design of multicycle operation of the Protein A resin, the optimal results show a decreasing trend until it reaches similar results as running at the slowest flow rate. However, optimization during the multicycle operation was able to achieve over 80% productivity in the use of Protein A resin, leading to better column design.

With the successful implementation of such an optimal strategy, we demonstrate that smaller designs can be used more efficiently while expecting savings in resins, buffers/water, and utilities that accompany productivity improvements.

ACKNOWLEDGEMENTS

The authors thank the Department of Chemical Engineering at Rowan University for their assistance in acquiring computational licenses and resources, and Purolite for providing the necessary data and testing the results predicted in this study.

REFERENCES

1. A. Puthenpurail, H. Rathi, S. M. Nauli, and A. Ally, "A Brief Synopsis of Monoclonal Antibody for the Treatment of Various Groups of Diseases.," 2022.
2. D. Stanton, "Protein A's mAb capture efficacy offsets cost, says GE launching new offering." www.biopharma-reporter.com, Sep. 26, 2017. [Online]. Available: https://www.biopharma-reporter.com/Article/2017/09/26/Protein-A-s-efficacy-offsets-cost-says-GE-as-it-launches-new-offering?utm_source=copyright&utm_medium=OnSite&utm_campaign=copyright
3. H. Motulsky and A. Christopoulos, *Fitting Models to Biological Data using Linear and Nonlinear Regression*. 2003.
4. F. Ghanem, S. S. Jerpoth, and K. M. Yenkie, "Improved Models for Chromate Removal Using Ion Exchangers in Drinking Water Applications," *J. Environ. Eng.*, vol. 148, no. 5, May 2022, doi: 10.1061/(ASCE)EE.1943-7870.0001997.
5. M. Korkmaz, C. Özmetin, E. Özmetin, and Y. Süzen, "Modelling of boron removal from solutions by ion exchange for column reactor design in boron mine wastewater treatment," *DESALINATION WATER Treat.*, vol. 179, pp. 63–74, 2020, doi: 10.5004/dwt.2020.25041.
6. I. M. Ross, *A primer on Pontryagin's principle in optimal control*, 2nd Edition. Collegiate Publishers, 2009. [Online]. Available: https://search.library.wisc.edu/catalog/9910894537702121
7. S. Misra, M. F. Wahab, D. C. Patel, and D. W. Armstrong, "The utility of statistical moments in chromatography using trapezoidal and Simpson's rules of peak integration," *J. Sep. Sci.*, vol. 42, no. 8, pp. 1644–1657, Apr. 2019, doi: 10.1002/jssc.201801131.
8. G. Carta, A. R. Ubiera, and T. M. Pabst, "Protein Mass Transfer Kinetics in Ion Exchange Media: Measurements and Interpretations," *Chem. Eng. Technol.*, vol. 28, no. 11, pp. 1252–1264, Nov. 2005, doi: 10.1002/ceat.200500122.
9. P. Hamill, *Lagrangians and Hamiltonians*, 4th printing. Cambridge University Press, 2018.
10. A. Staby, I. H. Jensen, and I. Mollerup, "Comparison of chromatographic ion-exchange resins I. Strong anion-exchange resins," *J Chromatogr A*, p. 13, 2000.
11. V. Rico-Ramireza and U. M. Diwekar, "Stochastic maximum principle for optimal control under uncertainty," *Comput. Chem. Eng.*, p. 5, 2004.
12. M. Hedhammar, A. E. Karlström, and S. Hober, *Chromatographic methods for protein purification*. AlbaNova University Center, Dept. of

Biotechnology, SE-106 91 Stockholm, Sweden: Royal Institute of Technology, 2006.
13. B. A. Patel *et al.*, "On-Line Ion Exchange Liquid Chromatography as a Process Analytical Technology for Monoclonal Antibody Characterization in Continuous Bioprocessing," *Anal. Chem.*, vol. 89, no. 21, pp. 11357–11365, Nov. 2017, doi: 10.1021/acs.analchem.7b02228.
14. J. Dawson, "A Review of Chromatography Methods for the Large Scale Downstream Protein Purification of Monoclonal Antibodies," 2019.
15. S. Engell and A. Toumi, "Optimisation and control of chromatography," *Comput. Chem. Eng.*, vol. 29, no. 6, pp. 1243–1252, May 2005, doi: 10.1016/j.compchemeng.2005.02.034.
16. S. Arora, B. V. Ayyar, and R. O'Kennedy, "Affinity Chromatography for Antibody Purification," in *Protein Downstream Processing*, vol. 1129, N. E. Labrou, Ed., in Methods in Molecular Biology, vol. 1129. , Totowa, NJ: Humana Press, 2014, pp. 497–516. doi: 10.1007/978-1-62703-977-2_35.
17. N. Kyurkchiev and S. Markov, "Sigmoidal Functions: Some Computational and Modelling Aspects," *Biomath Commun.*, vol. 1, no. 2, Mar. 2015, doi: 10.11145/j.bmc.2015.03.081.
18. E. R. Arenas-Flores *et al.*, "Treatment of a mining water effluent for the sorption of heavy metal ions using polymer composite beads in a continuous column," *Water Environ. J.*, p. wej.12710, Apr. 2021, doi: 10.1111/wej.12710.
19. S. Biswas and U. Mishra, "Continuous Fixed-Bed Column Study and Adsorption Modeling: Removal of Lead Ion from Aqueous Solution by Charcoal Originated from Chemical Carbonization of Rubber Wood Sawdust," *J. Chem.*, vol. 2015, pp. 1–9, 2015, doi: 10.1155/2015/907379.
20. A. Staby *et al.*, "Comparison of chromatographic ion-exchange resins," *J. Chromatogr. A*, vol. 1164, no. 1–2, pp. 82–94, Sep. 2007, doi: 10.1016/j.chroma.2007.06.048.
21. J. Luo, O. A. Cirpka, and P. K. Kitanidis, "Temporal-moment matching for truncated breakthrough curves for step or step-pulse injection," *Adv. Water Resour.*, vol. 29, no. 9, pp. 1306–1313, Sep. 2006, doi: 10.1016/j.advwatres.2005.10.005.
22. M. N. Goltz and P. V. Roberts, "Using the method of moments to analyze three-dimensional diffusion-limited solute transport from temporal and spatial perspectives," *Water Resour. Res.*, vol. 23, no. 8, pp. 1575–1585, Aug. 1987, doi: 10.1029/WR023i008p01575.
23. H. S. Fogler, "Residence Time Distributions of Chemical Reactors," in *Elements of chemical reaction engineering*, Fifth edition., Boston: Prentice Hall, 2016, pp. 767–806.
24. J. W. Jawitz, "Moments of truncated continuous univariate distributions," *Adv. Water Resour.*, vol. 27, no. 3, pp. 269–281, Mar. 2004, doi: 10.1016/j.advwatres.2003.12.002.
25. S. Abbasi and U. M. Diwekar, "Characterization and stochastic modeling of uncertainties in the biodiesel production," *Clean Technol. Environ. Policy*, vol. 16, pp. 79–94, Mar. 2013.
26. T. Szabados, "An elementary introduction to the Wiener process and stochastic integrals," *ArXiv10081510 Math*, Aug. 2010, Accessed: Feb. 21, 2021. [Online]. Available: http://arxiv.org/abs/1008.1510
27. D. T. Brereton, in *Stochastic Simulation of Processes, Fields and Structures*, Ulm University: Institute of Stochastics, 2014, pp. 108–121.
28. U. Diwekar, "Optimal Control and Dynamic Optimization," in *Introduction to Applied Optimization*, vol. 22, in Springer Optimization and Its Applications, vol. 22. , Boston, MA: Springer US, 2008, pp. 215–277. doi: 10.1007/978-0-387-76635-5.
29. K. M. Yenkie and U. Diwekar, "Stochastic Optimal Control of Seeded Batch Crystallizer Applying the Ito Process," *Ind. Eng. Chem. Res.*, pp. 108–122, Jun. 2012.
30. Z. Lei, C. Li, and B. Chen, "Extractive Distillation: A Review," *Sep. Purif. Rev.*, vol. 32, no. 2, pp. 121–213, Jan. 2003, doi: 10.1081/SPM-120026627.
31. P. Ravisankar, S. Anusha, K. Supriya, and U. A. Kumar, "Fundamental Chromatographic Parameters," *Int J Pharm Sci Rev Res*, vol. 55, no. 09, pp. 46–50, Apr. 2019.
32. J. Harmand, C. Lobry, A. Rapaport, and T. Sari, *Optimal Control in Bioprocesses: Pontryagin's Maximum Principle in Practice*, First Edition., vol. 3. Wiley, 2019.
33. Z. Artstein, "Pontryagin Maximum Principle Revisited with Feedbacks," *Eur. J. Control*, vol. 1, pp. 46–54, 2011.
34. L. C. Young, "Orthogonal collocation revisited," *Comput. Methods Appl. Mech. Eng.*, vol. 345, pp. 1033–1076, 2019, doi: https://doi.org/10.1016/j.cma.2018.10.019.
35. Santosh K Gupta, "Orthogonal Collocation (OC)," in *Numerical Methods for Engineers*, 3rd ed., New Age International (P) Limited, Publishers, 1995, pp. 229–246.
36. F. Ghanem and K. M. Yenkie, "Optimal Control of Chromate Removal via Enhanced Modeling using the Method of Moments," 2023. [Online]. Available: https://api.semanticscholar.org/CorpusID:259316597
37. S. Y. E, Y. Hu, R. Molden, H. Qiu, and N. Li, "Identification and Quantification of a Problematic

Host Cell Protein to Support Therapeutic Protein Development," *J. Pharm. Sci.*, vol. 112, no. 3, pp. 673–679, Mar. 2023, doi: 10.1016/j.xphs.2022.10.008.